Science of the Total Environment 948 (2024) 174856

Contents lists available at ScienceDirect

Science of the Total Environment

journal homepage: www.elsevier.com/locate/scitotenv

A kinetics-coupled multi-surface complexation model deciphering arsenic adsorption and mobility across soil types

Yutong Liu [a], Liyang Zhang [a], Yubo Wen [b], Hanzhao Zhai [a], Yuli Yuan [a], Chao Guo [a], Lei Wang [c,d], Fei Wu [e], Chengshuai Liu [e], Jian Xiao [f], Juan Liu [g], Xiaofan Yang [h], Yuanfeng Cai [a], Junfeng Ji [a], Yuanyuan Liu [a,*]

[a] Key Laboratory of Surficial Geochemistry (Ministry of Education), School of Earth Sciences and Engineering, Nanjing University, Nanjing 210023, China
[b] School of Geographical Science, Nantong University, Nantong, Jiangsu 226007, China
[c] Office of Land Quality Geochemical Assessment of Guangxi, Nanning, Guangxi 530023, China
[d] Geology Team No. 4 of Guangxi Zhuang Autonomic Region, Nanning, Guangxi 530031, China
[e] State Key Laboratory of Environmental Geochemistry, Institute of Geochemistry, Chinese Academy of Sciences, Guiyang 550081, China
[f] Key Laboratory of Agrometeorology of Jiangsu Province, School of Ecology and Applied Meteorology, Nanjing University of Information Science & Technology, Nanjing 210044, China
[g] Key Laboratory of Water and Sediment Sciences, College of Environmental Sciences and Engineering, Peking University, Beijing 100871, China
[h] State Key Laboratory of Earth Surface Processes and Resource Ecology, Faculty of Geographical Science, Beijing Normal University, Beijing, China

HIGHLIGHTS

- A model was developed to quantify As adsorbents and their contributions in soils.
- Fe oxides serve as the primary adsorbents at low As concentrations.
- At high As concentrations, clay mineral and soil OC become significant.
- Fe-rich clay enhances soil's resistance to As release under reduction condition.
- Mn oxides indirectly influence As adsorption by oxide As(III) to As(V).

GRAPHICAL ABSTRACT

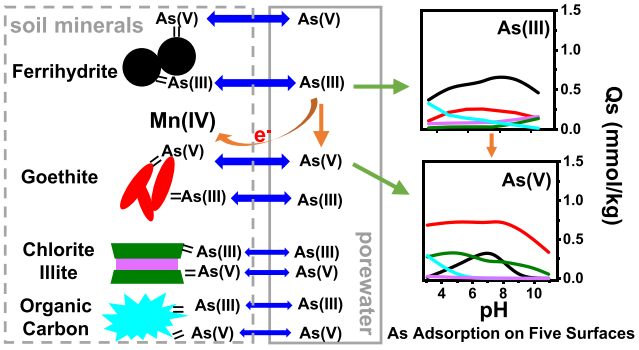

ARTICLE INFO

Editor: Bo Gao

Keywords:
Arsenic adsorption
Natural soils
Surface complexation model
Adsorption kinetics
Oxidation kinetics

ABSTRACT

The diversity of soil adsorbents for arsenic (As) and the often-overlooked influence of manganese (Mn) on As(III) oxidation impose challenges in predicting As adsorption in soils. This study uses Mössbauer spectroscopy, X-ray diffraction of oriented clay, and batch experiments to develop a kinetic coupled multi-surface complexation model that characterizes As adsorbents in natural soils and quantifies their contributions to As adsorption. The model integrates dynamic adsorption behaviors and Mn-oxide interactions with unified thermodynamic and kinetic parameters. The results indicate that As adsorption is governed by five primary adsorbents: poorly crystalline Fe oxides, well crystalline Fe oxides, Fe-rich clay, Fe-depletion clay, and organic carbon (OC). Fe oxides dominate As adsorption at low As concentrations. However, at higher As concentrations, soils from

* Corresponding author at: Nanjing University, Xianlin Ave. 163, Nanjing, Jiangsu, China.
E-mail address: yuanyuan.liu@nju.edu.cn (Y. Liu).

https://doi.org/10.1016/j.scitotenv.2024.174856
Received 9 May 2024; Received in revised form 2 July 2024; Accepted 16 July 2024
Available online 19 July 2024

carbonate strata, with higher content of Fe-rich clay, exhibit stronger As adsorption capabilities than soils from Quaternary sediment strata. The enrichment in Fe-rich clay can enhance the resistance of adsorbed As to reduction processes affecting Fe oxides. Additionally, extensive redox cycles in paddy fields increase OC levels, enhancing their As adsorption compared to upland fields. This model framework provides novel insights into the intricate dynamics of As within soils and a versatile tool for predicting As adsorption across diverse soils.

1. Introduction

Arsenic (As) is a hazardous element known to accumulate in soils as a result of natural processes such as the weathering of parental rocks and anthropogenic activities (Harvey et al., 2002; Koons et al., 1980; Smedley and Kinniburgh, 2002; Xiao et al., 2022). Various biogeochemical processes, including adsorption, ligand exchange, redox reaction, and precipitation, influence the retention, release and bioavailability of As in soils (Gillispie et al., 2015; Khan et al., 2010; Paikaray and Peiffer, 2022; Suda and Makino, 2016). Adsorption, in particular, plays a pivotal role in controlling As mobility and availability (Dixit and Hering, 2003). The adsorption of As on soils varies with soil compositions, which includes different Fe oxides, clay minerals, and organic carbon (OC) (Chi et al., 2021; Gimenez et al., 2007; Goldberg et al., 2005; Pedersen et al., 2006; Silva et al., 2010). Moreover, redox conditions profoundly impact the compositions and contents of Fe oxides, OC, and As, thereby affecting As adsorption behavior and potential mobilization (Scott and Morgan, 1995; Tufano et al., 2008).

Characterizing Fe oxides and clay minerals in soils are crucial for understanding As adsorption dynamics. Mössbauer spectroscopy and extended X-ray absorption fine structure (EXAFS) spectroscopy provide information on the phases of Fe in soils, but these spectral techniques require significant amount of Fe for effective signaling and are limited in revealing the accessibilities or reactivities of these minerals (Kaplan et al., 2016; Sjostedt et al., 2013). Conversely, sequential chemical extraction categorizes Fe based on its solubility and accessibility within the soil matrix, but it lacks phases-specific information (Wenzel et al., 2001). X-ray diffraction (XRD) is effective for identifying crystalline structures of clay minerals, providing insights into their mineral types and abundance (Moore and Reynolds, 1997). Combing these techniques will provide a comprehensive understanding of Fe oxide and clay mineral compositions, essential for understanding As adsorption in natural environments.

Furthermore, accurately quantifying the contributions of various adsorbents to As adsorption poses significant challenges. Surface complexation models (SCMs), widely used to describe ion adsorption, are integrated with the component additivity (CA) approach to predict ion adsorption in various soil types (Chi et al., 2021; Reich et al., 2010). For instance, Chi et al. implemented a CA-based SCM by lineally adding As(III) adsorption on various minerals, including Fe-minerals, illite, dolomite and soil OC (Chi et al., 2021). However, this model encountered challenges in accurately capturing some experimental results, partly because it neglected As(III) oxidation by Mn oxides and failed to capture the variability of As adsorbents within soils matrices. Furthermore, the application of CA-based SCM to As(V) adsorption remains inadequately explored.

This study developed a kinetic coupled multi−surface complexation model (MSCM), that integrates As(V) and As(III) adsorption dynamics with oxidation of As(III) by Mn oxides, based on Mössbauer spectroscopy, X-ray diffraction of oriented clay, and batch adsorption experiments conducted on soils from southwest China. This study identified the dominant reactive adsorption surfaces for As and elucidated their contributions for As adsorption in a broad range of soil types. This kinetic coupled MSCM framework not only advanced out knowledge of As interaction within soils but also offers a robust tool for predicting As mobility and bioavailability across heterogeneous soil landscapes.

2. Materials and methods

2.1. Soil sampling and sample preparation

Five paddy and upland soil samples were collected from three distinct locations in the karst regions of South China, each representing diverse soil origins (Fig. S1). The soils from Yunbiao Town (YB) are composed of Quaternary sediments deposited by the Zhenlong River. In contrast, the soils from Maling Town (ML) and Baisuo Town (BS) have developed directly on Devonian carbonate and Permian limestone strata, respectively (Wei et al., 2014). Details for soil sampling and preparation are provided in the supplementary information (SI). The soil samples were categorized based on their respective sampling sites and land usage types, denoted as YB-P, YB-U, ML-P, ML-U, and BS-P, where ‘P' represents paddy soils and ‘U' indicates upland soils.

2.2. Characterization of soil physical and chemical properties

The physical and chemical properties of the soil samples were analyzed. The analyses included determining particle size, specific surface area (SA), pH, water content, cation exchange capacities (CEC), total organic carbon (TOC), total inorganic carbon (TIC), and total soil contents of Ca, Mg, Al, Fe, Mn, and As. Detailed methodologies of these measurements are provided in the SI.

The clay particles (<2 μm in size) were isolated from each soil sample through Stokes' law for SA and X-ray diffraction (XRD) analyses (Moore and Reynolds, 1997). The XRD analyses were performed on oriented clay slides, both air-dried and treated with ethylene glycol solvation, to identify and quantify the clay mineralogy. Clay samples were first dispersed and pipetted onto glass slides, followed by a slow air-drying process to create natural oriented mounts. These mounts were then subjected to X-ray diffraction (XRD) analysis using a Rigaku D/MAX RAPID II diffractometer (Rigaku, Tokyo, Japan). The XRD parameters included Cu-Kα radiation, a 2θ range of 3° to 36° with a step size of 0.02°, and a counting time of 10 s per point, set at 40 kV and 100 mA. Following the initial XRD analysis, the air-dried clay slides were treated in ethylene glycol-saturated vapor for 46 h and before a second round of XRD analysis. The mineral composition of the clay samples was determined through both the air-dried and ethylene glycol-treated XRD data. The quantification of each clay mineral's content was performed on the air-dried slide data, using full pattern fitting with the TOPAS software package (Bruker, Germany) and Rietveld refinement method (Coelho, 2018).

A sequential chemical extraction method was modified from Wenzel's procedure to characterize Fe fractions and the associated As in the soil samples (SI) (Wenzel et al., 2001; Zhang et al., 2021). This modified procedure sequentially extracted amorphous and poorly crystalline Fe oxides (Fe_F1) and their associated As (As_F1), well crystalline Fe oxides (Fe_F2) and their associated As (As_F2), and (3) Fe and As combined with soil OC (Fe_F3 and As_F3) (Tessier et al., 1979). The residual Fe and As fractions (Fe_F4 and As_F4) were determined by subtracting the amounts of Fe and As in the extracted fractions from the total soil content.

A portion of the YB-P soil was treated with 0.2 M ammonium oxalate, separated by centrifugation, washed, and dried (YB-P_w/o F1). Then Mössbauer spectra of YB-P and YB-P_w/o F1 soil samples were collected at 12 K (somewhat similar to 4.2 K-liquid He temperature spectra) and recorded by a low-temperature closed-cycle Fe-57 Mössbauer

spectrometer (SLD-500/SHI-850-05, WissEl) to determine the iron mineralogy in these samples. In previous studies, 4.2 K spectra were generated to distinguish goethite from other oxides such as ferrihydrite, hematite, and clay Fe (Kaplan et al., 2016). The velocity of the Mössbauer spectra was calibrated by a standard α-iron foil. The spectral data were analyzed using MossWinn 4.0 (Klencsar, 2013).

2.3. As adsorption experiments

Four sets of batch experiments were conducted to investigate the adsorption behavior of As. The first set evaluated the adsorption kinetics of As(V) and As(III) in YB-P soils to determine the adsorption kinetic parameters and equilibrium times. The second set focused on As(V) adsorption in varied solution pH (pH envelopes) and initial As(V) concentration (adsorption isotherms) across five soil types, with the objective of identifying the active adsorption surfaces. The preference of As(V) over As(III) stemmed from As(V)'s stability against Mn oxidation. The third set explored As(III) adsorption in YB and ML soils through pH envelopes and adsorption isotherms. The fourth set investigated the influence of birnessite, introduced at 0.3 and 1.5 g/kg, on As(III) oxidation and adsorption dynamics within YB-P soils. In the fourth set, aqueous As(V) and As(III) speciation was determined using anion-exchange columns (LC-SAX) for their separation (Chiu and Hering, 2000). Details of the adsorption experiments and synthesis of birnessite are provided in the SI.

2.4. Kinetic coupled surface complexation modeling

A MSCM was firstly developed to describe As adsorption in natural soils. Total As adsorption in the soil is the cumulative sum of As(V) and As(III) adsorption on active surfaces including Fe oxides, clay minerals, and soil OC. As adsorption on Fe oxides and clay minerals was simulated using the diffuse double layer (DDL) model, that assumes two electrical layers extending from the surface to the bulk solution (Dzombak and Morel, 1990). The DDL model was selected for our multi-surface complexation model because previous studies have reported key parameters, such as equilibrium constants for both Fe minerals and clay minerals, for As adsorption using this model (Dixit and Hering, 2003; Dzombak and Morel, 1990; Manning and Goldberg, 1996; Zazzi et al., 2012). As adsorption on soil OC was simplified using equations based on As K-edge EXAFS results, which indicated As adsorption to natural OC through complexation with oxygen-containing functional groups (Biswas et al., 2019). The equations and parameters are provided in the SI.

Then the MSCM was coupled with redox and adsorption kinetics to describe dynamic As adsorption in natural soils. The kinetics of As(III) oxidation by Mn oxides (Eq. (1)) and the reduction of birnessite by soil OC (Eq. (2)) were described through second-order redox reactions (Eq. (3)):

$$MnO_{2(s)} + H_3AsO_{3(aq)} + H^+ \rightarrow Mn^{2+} + H_2AsO_4^- + H_2O \quad (1)$$

$$2MnO_{2(s)} + OC_{(s)} \rightarrow 2Mn^{2+} + CO_2 \quad (2)$$

$$R_j = k_j \prod_l C_l \quad (3)$$

where R_j (mmol/L) is the reaction rate of the second order redox reaction j, k_j (L/mmol)/h) is rate constant, and C_l (mmol/L) is the aqueous concentrations of species l. The kinetics of As adsorption and the variation in aqueous arsenic concentration were described using Eqs. (4) and (5):

$$\frac{\partial q_l^i}{\partial t} = \alpha_l^i \left(Q_l^i - q_l^i\right) \quad (4)$$

Table 1
Chemical and physical properties of soil samples.

Sample ID	pH	Water content (%)	CEC (cmol/kg)	TOC (%)	TIC (%)	SA (m^2/g)	SA of clay (m^2/g)	Major elements (%)				Mn (mg/kg)	As (mg/kg)	Particle size (%)				
								Ca	Mg	Al	Fe			1–2 (mm)	0.5–1	0.25–0.5	0.063–0.25	0.002–0.063	<0.002
YB-P	5.8	0.19	11.1	1.7	0.3	17.4	47.4	0.17	0.47	8.37	4.04	234.00	61.56	0.4	1.1	1.0	11.8	71.3	14.4
YB-U	6.2	0.14	5.2	0.4	0.2	10.5	51.5	0.18	0.23	7.36	2.47	309.24	60.84	0	0.4	2.9	20.4	65.2	11.1
ML-P	6.8	0.11	8.2	1.9	1.2	33.7	63.5	0.48	0.63	20.58	9.73	1667.49	120.50	0	1.0	5.0	7.4	59.3	27.3
ML-U	6.2	0.16	11.7	1.4	0.2	45.3	55.3	0.62	0.57	23.61	13.66	2216.44	175.52	0	0	0.2	6.4	57.2	36.2
BS-P	6.0	0.03	23.4	3.1	0.2	35.1	102.8	0.39	0.46	6.52	7.18	841.43	432.88	0	0.6	2.8	13.2	53.4	30.0

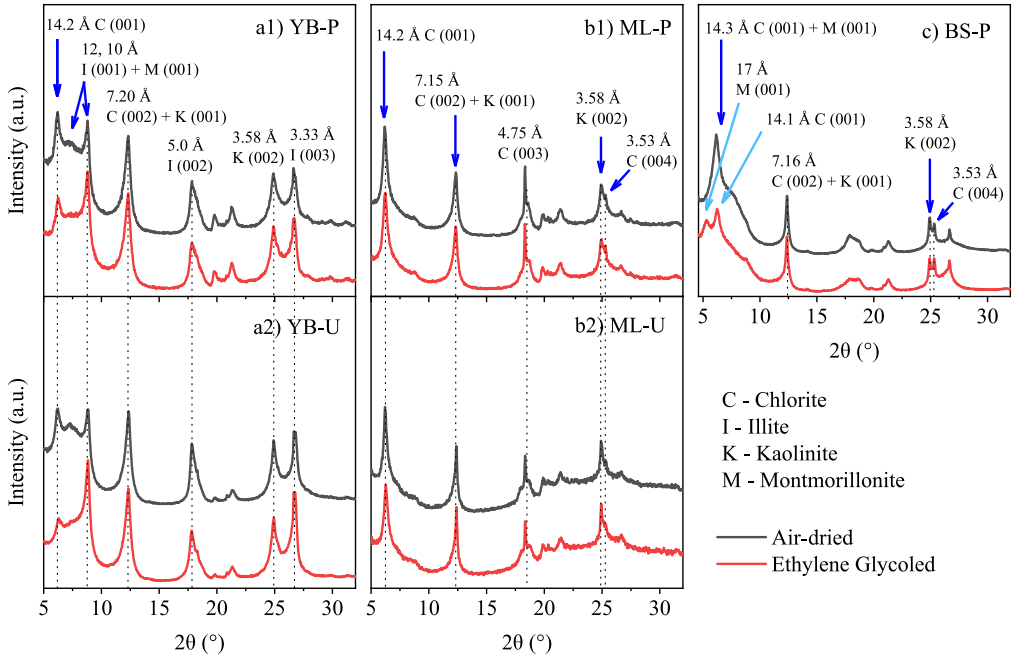

Fig. 1. XRD analysis of clay minerals in soil samples. The oriented clay slides were subjected to air drying (Air-dried) and ethylene glycol solvation treatment for 24 h (ethylene glycol).

$$\frac{\partial C_l}{\partial t} = \sum_j \gamma_{j,l} R_j - \sum_i \rho_s^i \alpha_l^i (Q_l^i - q_l^i) \quad (5)$$

where α_l^i (1/h) is rate constants, q_l^i and Q_l^i (mmol/g) are the adsorbed concentrations of species l on active surface i and that in equilibrium with aqueous solution, $\gamma_{j,l}$ is the stoichiometric coefficient of species l in reaction j, and ρ_s^i (g/L) is the solid concentration of surface i. The values of $Q_{i,l}$ is calculated with the MSCM.

The IPhreeqc geochemical module was coupled with MATLAB to solve the geochemical reactions and optimize parameters (Parkhurst and Appelo, 2013). The model input included initial concentrations of aqueous species (mmol/L), solid concentrations of different fractions (g/L), site densities (sites/nm^2), SAs (m^2/g), cation exchange sites (cmol/kg), and equilibrium and kinetic constants. Parameters were optimized to match the model-simulated results with experimental data. The goodness of fitting was evaluated by minimizing the root mean square relative error (RMSRE $= \sqrt{\sum_j^N \left(1 - C_j'/C_j\right)^2/(N-1)}$, where C' is the simulated value and N is the total number of samples).

2.5. Sensitivity analysis and uncertainty quantification

Sensitivity and uncertainty analyses were performed to evaluate the predictive accuracy of the MSCM. The Morris method was applied to identify the most influential parameters in the MSCM (Morris, 1991; Mr, 2014). Then, parameter error estimation was performed to obtain the variances of these parameters (σ) using a covariance matrix derived from the Jacobian matrix (Friedland, 1997; Liu and Zachara, 2001). The calculated variances were used to define the probability distribution of sensitive parameters, assuming a normal distribution. For uncertainty propagation from parameters to model predictions, Latin hypercube sampling, a Monte Carlo sampling method, was used to randomly draw 1000 sets of parameter combinations from the established probability distributions (Helton and Davis, 2003; Khan et al., 2008). This approach enabled the assessment of the model's predictive uncertainty, yielding average prediction and 95 % prediction interval from the 1000 simulation runs. The advanced Morris method, parameter error estimation, and uncertainty quantification were implemented in MATLAB, with details available in the SI.

3. Results and discussion

3.1. Soil properties reflecting the influence of soil origin and pedogenic processes

The chemical and physical properties of soil samples collected from different regions and soil usage types exhibited significant variability, reflecting the influence of soil origin and pedogenic processes (Table 1). As expected, soils developed from Devonian carbonate strata (ML) and Permian limestone strata (BS) were richer in Ca content compared to those derived from Quaternary sediments (YB). This is attributed to the long-term weathering of carbonate rocks, which not only led to higher clay contents but also tended to enrich insoluble metals, such as Fe and Mn, in ML and BS soils (Wei et al., 2014; Xiao et al., 2022). In terms of clay content, ML and BS soils had higher clay content (>27.3 %) and, consequently, a larger specific SA (>33.70 m^2/g) than YB soils. The SA of clay in BS soils was the largest, followed by ML and then YB soils. XRD results of clay minerals (Fig. 1 and Table S4) revealed that clay minerals in ML and BS soils predominantly comprised Fe-rich clay, such as chlorite and montmorillonite-chlorite (>82.93 % in ML soils and 60.77 % in BS soil), with smaller proportions of illite and kaolinite. In contrast, Fe-depletion clay, such as illite and kaolinite, was the dominant clay minerals in YB soils (>92.0 %), accompanied by lesser amounts of chlorite. Furthermore, TOC concentrations were generally higher in paddy soils compared to upland soils within the same region, probably attributable to agricultural activities. The CEC ranged from 4.46 to 23.41 cmol/kg, influenced primarily by charged carboxyl groups in soil organic matter and sites on clay minerals (Liang et al., 2006; Parfitt et al., 1995).

3.2. The occurrence states of soil Fe and As and potential active adsorption surfaces in soils

The occurrence states of Fe and As in various soil samples were characterized using the modified sequential chemical extraction method (Table S5). The most abundant fractions in all soils were residual Fe and

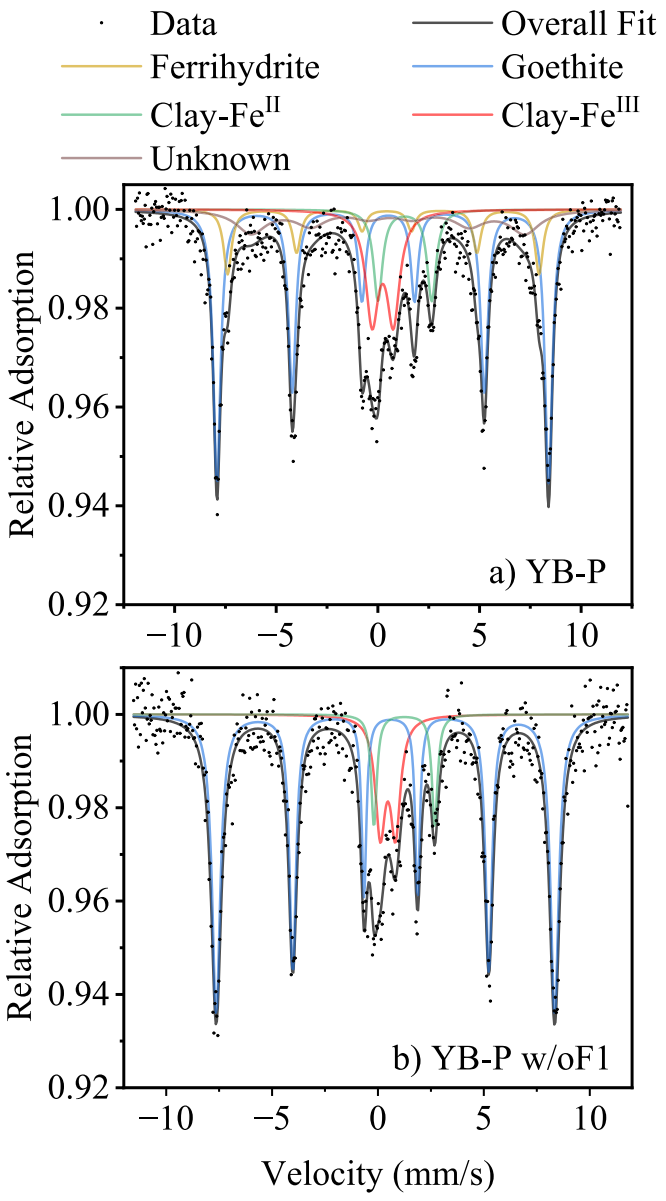

Fig. 2. Mössbauer spectra for YB-P soils before (a) and after the removal of fraction F1 (b).

As (Fe_F4 and As_F4), especially in soils developed from carbonate strata. Paddy soils exhibited higher Fe_F1 content than upland soils within the same region, probably due to redox cycles of Fe induced by the alternating flood and drought management practices typical of paddy fields (Jiang et al., 2017). Furthermore, both Fe and As were effectively extracted using the OC extraction solution (Fe_F3 and As_F3), indicating that Fe likely coprecipitated with OC in these soils. The extracted As (As_F3) also suggested its potential to form complexes with OC through ternary complexes comprising Fe, As and OC (Mikutta and Kretzschmar, 2011) and/or through complexes with the oxygen-containing functional groups of OC (Biswas et al., 2019).

Mössbauer spectroscopy provided insight into Fe phases in the YB-P and YB-P_w/o F1 soils (Fig. 2), with percentage contents estimated from corresponding peak areas (Table S6) (Stevens et al., 2005). Five major Fe species were identified in the YB-P soil: ferrihydrite, goethite, clay-bound Fe(III) (clay-Fe^{III}), clay-bound Fe(^{II}) (clay-Fe^{II}), and an unknown phase, which was likely OC-bound Fe, as suggested by its lower magnetic hyperfine field compared to ferrihydrite (Schwertmann et al., 2005). A comparative analysis of the Mössbauer spectra between the YB-P and YB-P_w/o F1 soils revealed the absence of ferrihydrite and OC-bound Fe after ammonium oxalate extraction. However, the mass balance calculations in Table S6 indicated a noticeable increase in goethite content in the YB-P_w/o F1 soil (15.50 %), approximately equal to the amount of OC-bound Fe in the YB-P soil (16.03 %). This observation suggested that OC-bound Fe may have been misinterpreted as goethite in the Mössbauer spectrum of the YB-P_w/o F1 soil, an inference supported by the variation in isomer shift values between the two soil samples (0.37 vs. 0.48). The variation in isomer shift indicated a potential change in the local environment of Fe atoms, possibly influenced by the removal of certain Fe phases or changes in Fe speciation after ammonium oxalate extraction.

The mass balance calculations from the sequential chemical extractions of Fe fractions (Table S5) and the quantification of Fe phases through Mössbauer spectroscopy (Table S6) suggested that Fe_F1 predominantly composed of ferrihydrite, with minor contributions from OC- and clay-bound Fe. Fe_F2 contained approximately half of the goethite, Fe_F3 consisted of a portion of OC-bound Fe, and Fe_F4 included non-extractable goethite along with OC- and clay-bound Fe. The sequential extraction method not only effectively categorized Fe oxides into groups with distinct adsorption properties, but also accounted for the accessibility of these Fe phases, notably the non-extractability of some goethite, OC- and clay-bound Fe. It's proven to be a valuable technique for quantifying the active adsorption surfaces of Fe oxides in natural soils.

3.3. As adsorption on soils and the influence of Mn oxides on As(III) adsorption

The pH envelopes and adsorption isotherms for As(V) across the five soil types are shown in Figs. 3 and 4. As(V) adsorption capacities varied significantly among the soils: BS-P exhibited the highest capacity, markedly exceeding ML-P, ML-U, and YB-P, all of which were considerably higher than YB-U (Fig. 3a2–e2). A similar trend was observed in As(III) adsorption, where adsorption capacities of ML-P, ML-U, and YB-P were significantly higher than YB-U (Fig. 3a4 and b4 and Fig. 4c2 and d2). The variation in adsorption capacities correlated with the distinct contents of active Fe fractions, TOC, and Fe-rich clays in each soil (Tables 1, S4 and S5).

As(V) adsorption generally decreased rapidly with pH under alkaline conditions across most soils, except for BS-P (Fig. 3a1–e1). The rapid decrease is attributed to the predominance of less adsorptive $HAsO_4^{2-}$ species under alkaline conditions (Goldberg and Suarez, 2013). However, BS-P soil demonstrated a slower decline in As(V) adsorption at high pH, probably due to its abundant adsorption sites. Previous studies supported that As(V) adsorption in Fe-rich soils exhibited less pH sensitivity (Goldberg et al., 2005). As(III) adsorption showed a typical pH envelope pattern in YB soils, with adsorption peak occurring near neutral pH (Fig. 3a3 and b3) (Goldberg, 2002). In contrast, the pH envelopes of As(III) in ML soils resembled those of As(V) (Fig. 4c1 and d1), suggesting potential oxidation of As(III) by Mn oxides, which are more prevalent in ML than YB soils.

To evaluate the impact of Mn oxides on As(III) adsorption, birnessite was added to YB-P soil at concentrations of 0.3 and 1.5 g/kg prior to pH envelope experiments (Fig. 4a and b). The experimental results showed the presence of As(V) in the aqueous solution, with higher aqueous As (V) concentration corresponding to higher birnessite concentration. The pH envelopes thus closely resembled those typical for As(V) adsorption, characterized by enhanced As adsorption under acidic conditions and a rapid decrease under alkaline conditions. This proved that birnessite facilitated the oxidation of As(III) to As(V), thereby influencing its adsorption dynamics.

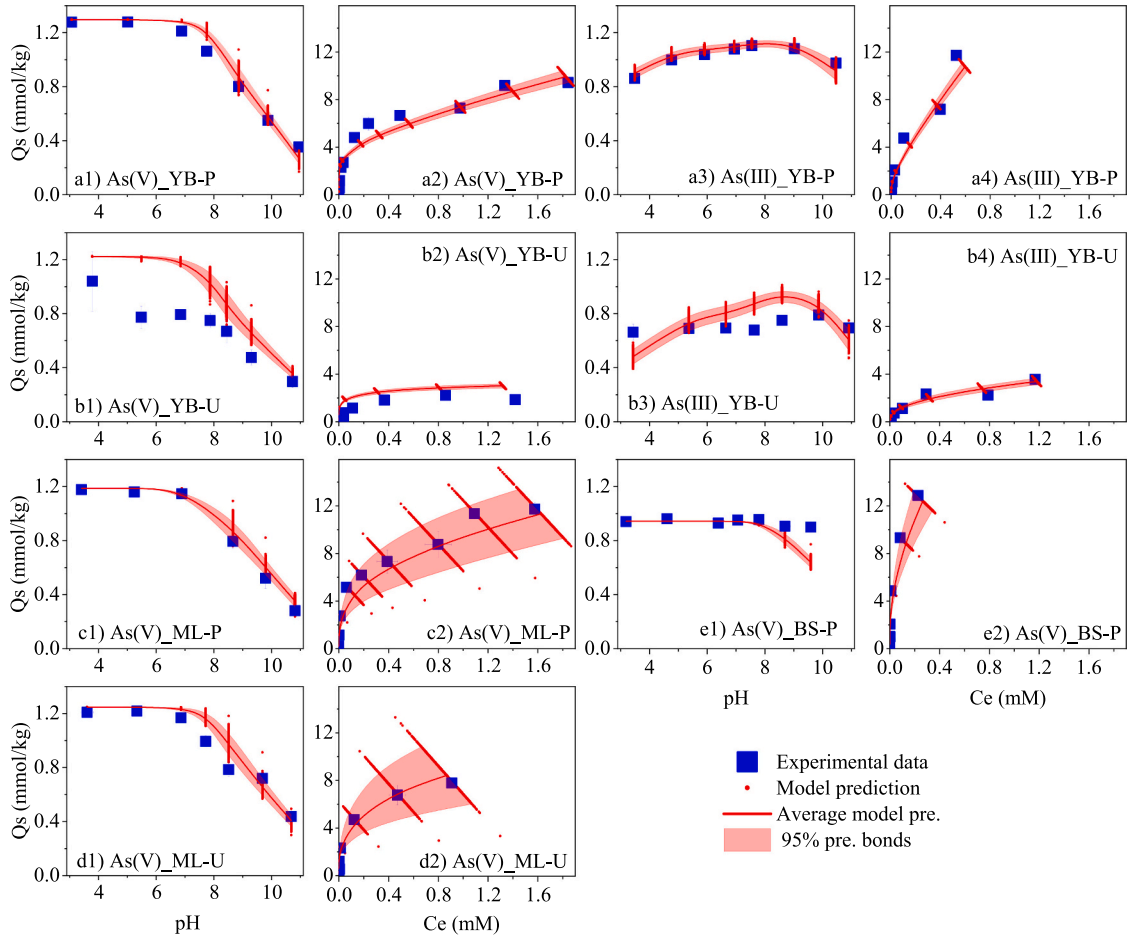

Fig. 3. The pH envelopes (a1–e1, a3 and b3) and adsorption isotherms (a2–e2, a4 and b4) of As(V) and As(III) adsorption on different soils at 25 ± 2 °C. The initial As concentration for pH envelops was 0.1 mM, and the pH for adsorption isotherms was fixed at 7.00 ± 0.20. The symbols are experimental data, error bars represent the standard deviation from triplicate experiments, the red dots are predicted results from 1000 runs, the red lines are average results of the 1000 runs, and the red region represents the 95 % prediction bound, assuming that the results were independent and followed a normal distribution.

3.4. Development of the kinetic coupled MSCM for dynamic As adsorption

We initially developed a MSCM for As(V) and As(III) adsorption separately. Considering the influence of Mn oxide on As(III) adsorption, the MSCM was applied to analyze pH envelopes and adsorption isotherms for As(V) across the five soils to identify the active adsorption surfaces. The MSCM integrated various Fe fractions, clay fractions, and OC content to match the experimental observations. Ultimately, five active adsorption surfaces were selected for the MSCM due to their ability to uniformly fit all experimental results with the same set of parameters (Fig. 3). These surfaces were characterized as follows: Fe_F1 primarily represented by ferrihydrite, Fe_F2 by goethite, Fe-rich clay by chlorite, Fe-depletion clay by illite, and soil OC quantified by TOC. To minimize reliance on empirical fitting, most model parameters were experimentally measured or adopted from studies on pure minerals (Table 2). Parameter adjustments were performed only for SA for Fe_F1 and Fe_F2 (SA_1 and SA_2), site densities for Fe-rich clay and Fe-depletion clay ($N_{s,3}$ and $N_{s,4}$), and equilibrium constant for OC ($K_{5,As(V)}$). Subsequently, adsorption equilibrium constants for As(III) ($K_{i,\ As(III)}$) were derived through parameter fitting using pH envelopes and adsorption isotherms for As(III) in YB soils, which are characterized by low Mn content (Fig. 3).

To evaluate the reliability and predictive accuracy of the MSCM, sensitivity and uncertainty analyses were undertaken. The sensitivity analysis was conducted to identify the most influential parameters. Given the inherent sensitivity of adsorption sites, the sensitivity analysis only applied on equilibrium constants (Fig. S3). Out of 30 tested parameters, 13 with elementary effects exceeding 1.5 were selected for further uncertainty analysis. The variances of these 13 equilibrium constants, along with 4 parameters related to the number of adsorption sites (SA_1, SA_2, $N_{s,3}$ and $N_{s,4}$), were evaluated using their covariance matrix. These variances enabled the propagation of uncertainty from experimental measurements through parameters to model predictions.

The results demonstrated that the MSCM successfully captured the experimental results (Fig. 3), with all variances for these 17 sensitive parameters remaining within acceptable ranges (Table S7), confirming the robustness of the model's predictions. Although the model tended to slightly overestimate As(V) adsorption on YB-U soil under acid conditions (Fig. 3b1) and As(III) adsorption on YB-U soil at pH 7 to 9 (Fig. 3b3), these discrepancies were relatively small. Additionally, the broad 95 % prediction intervals observed in the adsorption isotherms for ML-P and ML-U soils were primarily due to variability in the site density of the Fe-rich clay. These minor variances are likely due to the model's simplification of soil adsorbents into five distinct active adsorption surfaces. While this simplification greatly facilitates practical application of the MSCM, it may introduce slight biases. Each adsorption surface still encompasses a mixture of various forms of amorphous Fe oxides, crystalline Fe oxides, and clay minerals, each with unique As adsorption properties (Carlson et al., 2002). This inherent complexity within each surface category is not fully captured in the MSCM framework. Despite these limitations, the overall performance of the MSCM

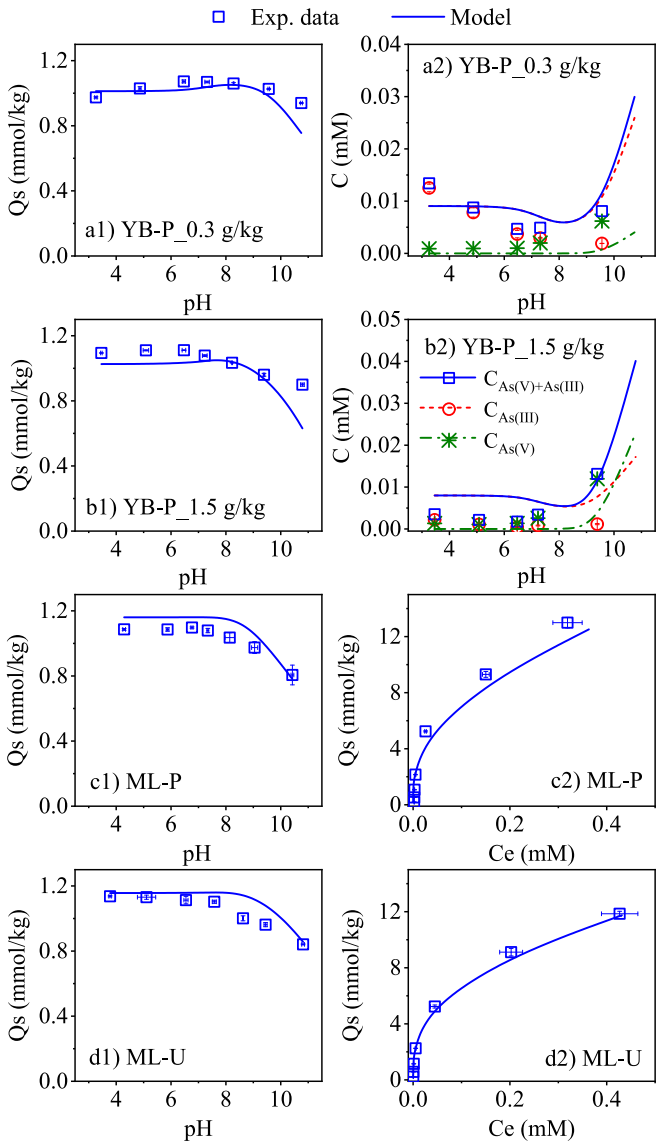

Fig. 4. The pH envelopes (a1–d1) and adsorption isotherms (c2 and d2) of As (III) adsorption on YB-P soils in the presence of 0.3 and 1.5 g/kg birnessite and on ML soils at 25 ± 2 °C.

exhibits its reliability and the potential to accurately predict As adsorption across diverse soil environments.

Subsequent to establishing the MSCM, it was integrated with kinetics processes to accurately predict As(III) adsorption in soils rich in Mn oxides. Adsorption kinetic parameters for As(V) and As(III) interactions with Fe oxides, clay minerals, and OC were derived from experiments conducted in YB-P soil (Fig. S4 and Table 2). Oxidation kinetics for As (III) by Mn oxides were then determined from experiments in YB-P soils in the presence of birnessite and in ML soils, maintaining all other parameters constant (Fig. 4 and Table 2). This comprehensive approach ensures that the MSCM accurately reflects the dynamic adsorption processes in varied soil environments, as detailed in the SI.

3.5. Adsorption dynamics of As in natural soils

Carbonate strata-derived soils contain higher levels of Mn oxides, capable of oxidizing As(III) to As(V), thereby influencing As adsorption dynamics. As(III) oxidation activities of naturally occurring Mn oxides in ML-P soil was similar to freshly prepared birnessite used in experiments with YB-P soil, whereas the oxidation in ML-U soil was notably slower

Table 2
Parameters for the kinetic coupled MSCM.

Parameters		Value	Reference
Thermo-dynamic parameters	[log $K_{1,+}$, log $K_{1,-}$]	[7.29, −8.93[d]]	[7.29, −8.93] (Dzombak and Morel, 1990)
	[log $K^{1,2,3}_{1,\ As(V)}$]	[8.67, 2.99, −4.70]	[8.67, 2.99, −4.70] (Dzombak and Morel, 1990)
	[log $K_{1,\ As(III)}$ ^{1,2}][b]	[3.52, −2.97[d]]	[4.02, −2.87] (Dixit and Hering, 2003)
	SA_1 (m^2/g)[b]	100[d]	40–110 (Stolze et al., 2019)
	$N_{s,1}$ (sites/nm^2)	2.3	2.3 (Goldberg and Johnston, 2001)
	[log $K_{2,+}$, log $K_{2,-}$]	[7.47, −9.51[d]]	[7.47, −9.51] (Dixit and Hering, 2003)
	[log $K_{2,\ As(V)}$ ^{1,2,3}]	[10.40, 6.21[d], −0.38]	[10.40, 6.21, −0.38] (Dixit and Hering, 2003)
	[log $K_{2,\ As(III)}$ ^{1,2}][b]	[3.00, −3.54[d]]	[5.19, −2.34] (Dixit and Hering, 2003)
	SA_2 (m^2/g)[b]	40[d]	40–110 (Stolze et al., 2019)
	$N_{s,2}$ (sites/nm^2)	2.3	2.3 (Goldberg and Johnston, 2001)
	[log $K_{3,+}$, log $K_{3,-}$]	[5.60, −8.20]	[5.60, −8.20] (Zazzi et al., 2012)
	[log $K_{3,\ As(V)}$ ^{1,2,3}][a]	[8.50[d], 2.50[d], −4.55]	
	[log $K_{3,\ As(III)}$ ^{1,2}][b]	[4.49, −1.85]	[4.49, −1.85] (Manning and Goldberg, 1997)
	SA_3 (m^2/g)	[c]	
	$N_{s,3}$ (sites/nm^2)[b]	0.3[d]	0.028–1.37 (Gu, 2006; Manning and Goldberg, 1997)
	[log $K_{4,+}$, log $K_{4,-}$]	[6.00, −10.50]	[6.00, −10.50] (Manning and Goldberg, 1996)
	[log $K_{4,\ As(V)}$ ^{1,2,3}]	[9.24[d], 3.66[d], −4.35[d]]	[9.24, 3.66, −4.35] (Manning and Goldberg, 1997)
	[log $K_{4,\ As(III)}$ ^{1,2}][b]	[3.25[d], −4.85]	[4.49, −1.85] (Manning and Goldberg, 1997)
	SA_4 (m^2/g)	[c]	
	$N_{s,4}$ (sites/nm^2)[b]	0.18[d]	0.028–1.37 (Gu, 2006; Manning and Goldberg, 1997)
	log $K_{5,\ As(V)}$[b]	9.45[d]	3.7 (Buschmann et al., 2006)
	log $K_{5,\ As(III)}$[b]	1.90[d]	0.40–1.01 (Biswas et al., 2019)
Kinetic parameters[b]	$\alpha_{Fe,As(V)}$ (1/h)	12.5	
	$\alpha_{Fe,As(III)}$ (1/h)	7.5	
	$\alpha_{clay,As(V)}$ (1/h)	0.15	
	$\alpha_{clay,As(III)}$ (1/h)	0.15	
	$k_{birnessite\_As(III)}$ (L/mmol/h)	0.1	0.11–0.27 (Oscarson et al., 1983; Scott and Morgan, 1995)
	$k_{birnessite\_SOC}$ (L/mmol/h)	0.001	
	$k_{Mn\_As(III)\_ML\text{-}P}$ (L/mmol/h)	0.1	
	$k_{Mn\_As(III)\_ML\text{-}U}$ (L/mmol/h)	0.03	

[a] The values were derived from modeling As(V) adsorption on chlorite (Fig. S2).
[b] The values were fitted from the experimental results.
[c] The SA values of clay were experimentally determined and are listed in Table 1.
[d] Sensitive parameters.

(Table 2). This variation is linked to the presence of Fe-Mn nodules in the ML area, which are significantly smaller in paddy fields than in upland fields due to extensive agricultural activities. These differences in Mn oxide levels and their reactivity toward As(III) across various soil types highlight the environmental and pedological influences on As

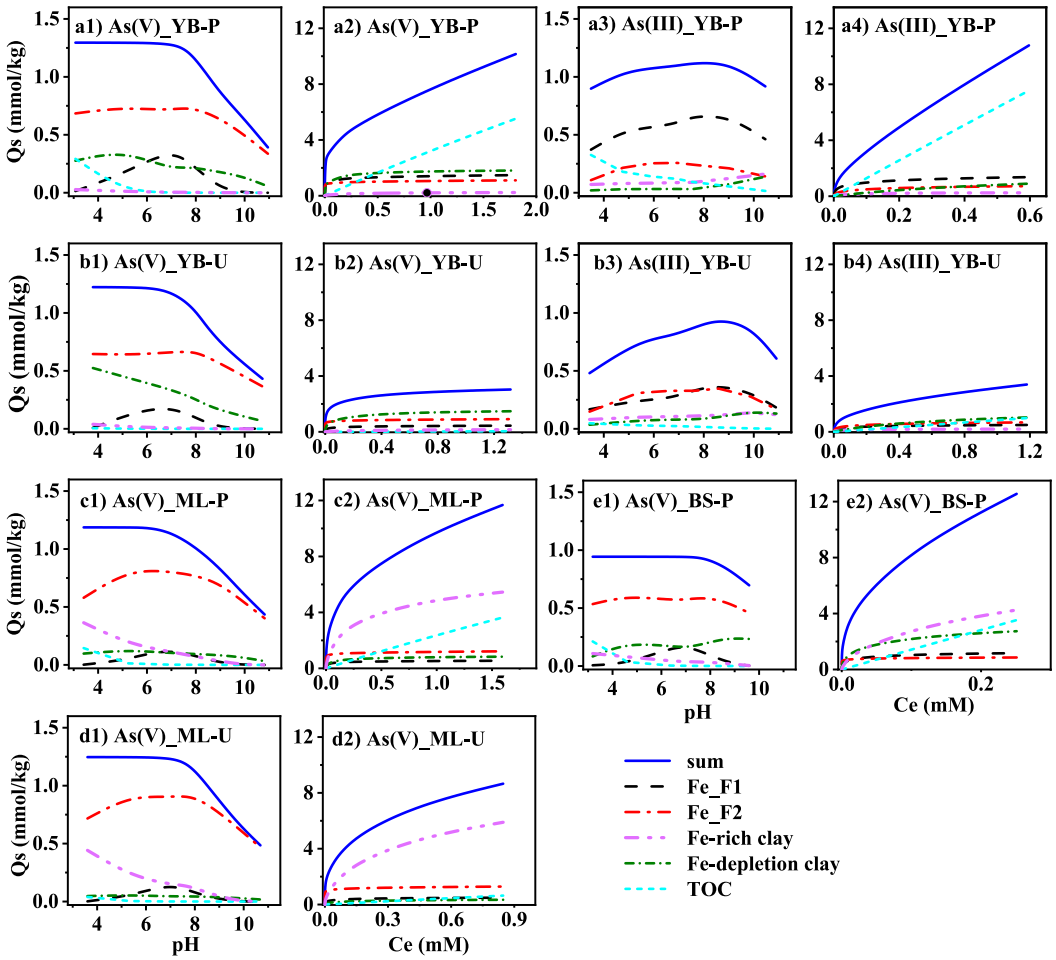

Fig. 5. Modeled contribution of active adsorption surfaces to the adsorption of As(V) on the YB-P (a), YB-U (b), ML-P (c), ML-U (d), and BS-P (e) soils, as well as As (III) adsorption on the YB-P (a3 and a4) and YB-U (b3 and b4) soils.

adsorption dynamics.

The adsorption kinetics of As(V) and As(III) on Fe oxides and clay minerals reveal distinctive patterns influenced by their chemical and structural properties (Table 2). The rate constant for As(V) adsorption on Fe oxides is higher than for As(III). This faster rate is due to the favorable electrostatic interactions between negatively charged As(V) species and positively charged sites on Fe oxides. Conversely, the adsorption rate constants for As(V) and As(III) on clay minerals are comparable, reflecting the influence of structural characteristics of clay minerals. The kinetic limitations imposed by the layered structure of clay minerals result in significantly lower rate constants compared to those for Fe oxides.

The contributions of various active surfaces elucidate the dynamic nature of As adsorption across diverse soil types (Fig. 5). The pH-dependence of As adsorption is primarily controlled by deprotonation of surfaces Fe_F1 and Fe_F2, as indicated by the sensitivity of constants $K_{1,-}$ and $K_{2,-}$. Fe_F2 is the dominant contributor to As adsorption at lower As concentrations, while Fe_F1 also playing significant roles in As(III) adsorption. As the adsorption capacity of Fe oxides reaches saturation, clay minerals, abundant in soil matrix, become critical adsorptive sites. Subsequently, OC plays an increasingly vital role, particularly in paddy soils, of which TOC content is higher than upland soils.

Soil origin and agricultural practices significantly influence the occurrence and mobility of As. Soils derived from carbonate strata typically contain higher total As concentrations, yet a significant portion exists in a residual form (As_F4). As a result, the mobilizable fractions of As (As_F1, As_F2, and As_F3) do not differ significantly between soils from carbonate strata and those from Quaternary sediment strata, nor between paddy and upland soils. When these mobilizable As fractions are released into soil pore water under reducing conditions, their fate is governed by adsorption processes. Soils from carbonate strata, richer in Fe-rich clay minerals, are expected to exhibit stronger As adsorption capabilities under such conditions compared to soils from Quaternary sediment strata. This difference in adsorption surfaces would inevitably influence the mobility and bioavailability of As.

4. Conclusion

The study has established a framework for understanding the complex interactions between soil characteristics and As adsorption, through a kinetic coupled MSCM. This model demonstrates that As adsorption in natural soils can be effectively predicted using a component additive approach. By considering the physical and chemical properties of different soil types, the model can be applied across various soils. This study also illustrates the significant effects of soil origin and agricultural practices on As mobility and bioavailability—key factors for assessing and managing As contamination under diverse environmental conditions. Particularly, the model highlights the critical roles of Fe-rich clays and OC in adsorbing As, especially under the reducing conditions typically found in paddy fields. Given its capability to integrate various geochemical interactions and adapt to different soil matrices, the model proves extremely valuable for environmental risk assessments and remediation strategies.

CRediT authorship contribution statement

Yutong Liu: Writing – review & editing, Writing – original draft, Software, Methodology, Formal analysis, Data curation. **Liyang Zhang:** Data curation. **Yubo Wen:** Resources. **Hanzhao Zhai:** Methodology. **Yuli Yuan:** Methodology. **Chao Guo:** Resources. **Lei Wang:** Resources. **Fei Wu:** Methodology. **Chengshuai Liu:** Methodology, Conceptualization. **Jian Xiao:** Methodology. **Juan Liu:** Investigation. **Xiaofan Yang:** Methodology. **Yuanfeng Cai:** Methodology. **Junfeng Ji:** Validation, Resources, Project administration. **Yuanyuan Liu:** Writing – review & editing, Supervision, Investigation, Funding acquisition, Conceptualization.

Declaration of competing interest

The authors declare that they have no known competing financial interests or personal relationships that could have appeared to influence the work reported in this paper.

Data availability

Data will be made available on request.

Acknowledgments

This research is funded by the National Natural Science Foundation of China (Grant No. 42273054, 42107027), the National Key Research and Development Project of the Ministry of Science and Technology of the People's Republic of China (Grant No. 2017YFD0800300), Jiangsu 'Double Innovation Plan', and Ecological and geochemical survey and study on the heavy metals in typical soil of Guangxi, China. We acknowledge the Center for Advanced Mössbauer Spectroscopy, Mössbauer Effect Data Center, Dalian Institute of Chemical Physics, CAS, for providing the Mössbauer measurement and analysis.

Appendix A. Supplementary data

The Supplementary Information is available free of charge, including details of methods, model parameters, and some experimental results. Supplementary data to this article can be found online at https://doi.org/10.1016/j.scitotenv.2024.174856.

References

Biswas, A., Besold, J., Sjosted, C., Gustafsson, J.P., Scheinost, A.C., Planer-Friedrich, B., 2019. Complexation of arsenite, arsenate, and monothioarsenate with oxygen-containing functional groups of natural organic matter: an XAS study. Environ. Sci. Technol. 53 (18), 10723–10731.
Buschmann, J., Kappeler, A., Lindauer, U., Kistler, D., Berg, M., Sigg, L., 2006. Arsenite and arsenate binding to dissolved humic acids: influence of pH, type of humic acid, and aluminum. Environ. Sci. Technol. 40 (19), 6015–6020.
Carlson, L., Bigham, J.M., Schwertmann, U., Kyek, A., Wagner, F., 2002. Scavenging of as from acid mine drainage by schwertmannite and ferrihydrite: a comparison with synthetic analogues. Environ. Sci. Technol. 36 (8), 1712–1719.
Chi, Z., Xie, X., Pi, K., Wang, Y., 2021. Mineralogical controls on arsenite adsorption onto soils: batch experiments and model-based quantification. Sci. Total Environ. 767, 144920.
Chiu, V.Q., Hering, J.G., 2000. Arsenic adsorption and oxidation at manganite surfaces. 1. Method for simultaneous determination of adsorbed and dissolved arsenic species. Environ. Sci. Technol. 34 (10), 2029–2034.
Coelho, A.A., 2018. TOPAS and TOPAS-academic: an optimization program integrating computer algebra and crystallographic objects written in C++. J. Appl. Cryst. 51 (1), 210–218.
Dixit, S., Hering, J.G., 2003. Comparison of arsenic(V) and arsenic(III) sorption onto iron oxide minerals: implications for arsenic mobility. Environ. Sci. Technol. 37 (18), 4182–4189.
Dzombak, D.A., Morel, F.M.M., 1990. Surface Complexation Modeling: Hydrous Ferric Oxide. John Wiley & Sons, New York.
Friedland, B., 1997. A nonlinear observer for estimating parameters in dynamic systems. Automatica 33 (8), 1525–1530.
Gillispie, E.C., Sowers, T.D., Duckworth, O.W., Polizzotto, M.L., 2015. Soil pollution due to irrigation with arsenic-contaminated groundwater: current state of science. Curr. Pollut. Rep. 1 (1), 1–12.
Gimenez, J., Martinez, M., de Pablo, J., Rovira, M., Duro, L., 2007. Arsenic sorption onto natural hematite, magnetite, and goethite. J. Hazard. Mater. 141 (3), 575–580.
Goldberg, S., 2002. Competitive adsorption of arsenate and arsenite on oxides and clay minerals. Soil Sci. Soc. Am. J. 66 (2), 413–421.
Goldberg, S., Johnston, C.T., 2001. Mechanisms of arsenic adsorption on amorphous oxides evaluated using macroscopic measurements, vibrational spectroscopy, and surface complexation modeling. J. Colloid Interface Sci. 234 (1), 204–216.
Goldberg, S., Suarez, D.L., 2013. Arsenate adsorption by unsaturated alluvial sediments. Soil Sci. Soc. Am. J. 77 (3), 782–791.
Goldberg, S., Lesch, S.M., Suarez, D.L., Basta, N.T., 2005. Predicting arsenate adsorption by soils using soil chemical parameters in the constant capacitance model. Soil Sci. Soc. Am. J. 69 (5), 1389–1398.
Gu, X., 2006. Surface Complexation Modelling of Heavy Metal Adsorption onto Natural Clay Minerals. University of Guelph.
Harvey, C.F., Swartz, C.H., Badruzzaman, A.B.M., Keon-Blute, N., Yu, W., Ali, M.A., Jay, J., Beckie, R., Niedan, V., Brabander, D., Oates, P.M., Ashfaque, K.N., Islam, S., Hemond, H.F., Ahmed, M.F., 2002. Arsenic mobility and groundwater extraction in Bangladesh. Science 298 (5598), 1602–1606.
Helton, J.C., Davis, F.J., 2003. Latin hypercube sampling and the propagation of uncertainty in analyses of complex systems. Reliab. Eng. Syst. Saf. 81 (1), 23–69.
Jiang, J., Dai, Z., Sun, R., Zhao, Z., Dong, Y., Hong, Z., Xu, R., 2017. Evaluation of ferrolysis in arsenate adsorption on the paddy soil derived from an Oxisol. Chemosphere 179, 232–241.
Kaplan, D.I., Kukkadapu, R., Seaman, J.C., Arey, B.W., Dohnalkova, A.C., Buettner, S., Li, D., Varga, T., Scheckel, K.G., Jaffe, P.R., 2016. Iron mineralogy and uranium-binding environment in the rhizosphere of a wetland soil. Sci. Total Environ. 569, 53–64.
Khan, A.A., Lye, L., Husain, T., 2008. Latin hypercube sampling for uncertainty analysis in multiphase modelling. J. Environ. Eng. Sci. 7 (6), 617–626.
Khan, M.A., Stroud, J.L., Zhu, Y.G., McGrath, S.P., Zhao, F.J., 2010. Arsenic bioavailability to rice is elevated in Bangladeshi paddy soils. Environ. Sci. Technol. 44 (22), 8515–8521.
Klencsar, Z., 2013. MossWinn-methodological advances in the field of Mossbauer data analysis. Hyperfine Interact. 217 (1–3), 117–126.
Koons, R.D., Helmke, P.A., Jackson, M.L., 1980. Association of trace-elements with iron-oxides during rock weathering. Soil Sci. Soc. Am. J. 44 (1), 155–159.
Liang, B., Lehmann, J., Solomon, D., Kinyangi, J., Grossman, J., O'Neill, B., Skjemstad, J. O., Thies, J., Luizao, F.J., Petersen, J., Neves, E.G., 2006. Black carbon increases cation exchange capacity in soils. Soil Sci. Soc. Am. J. 70 (5), 1719–1730.
Liu, C.X., Zachara, J.M., 2001. Uncertainties of monod kinetic parameters nonlinearly estimated from batch experiments. Environ. Sci. Technol. 35 (1), 133–141.
Manning, B.A., Goldberg, S., 1996. Modeling arsenate competitive adsorption on kaolinite, montmorillonite and illite. Clay Clay Miner. 44 (5), 609–623.
Manning, B.A., Goldberg, S., 1997. Adsorption and stability of arsenic(III) at the clay mineral-water interface. Environ. Sci. Technol. 31 (7), 2005–2011.
Mikutta, C., Kretzschmar, R., 2011. Spectroscopic evidence for ternary complex formation between arsenate and ferric iron complexes of humic substances. Environ. Sci. Technol. 45 (22), 9550–9557.
Moore, D.M., Reynolds, R.C.J., 1997. X-Ray Diffraction and the Identification and Analysis of Clay Minerals. Oxford University Press, New York.
Morris, M.D., 1991. Factorial sampling plans for preliminary computational experiments. Technometrics 33 (2), 161–174.
Mr, 2014. Sensitivity Analysis-Morris Method (Advanced). MATLAB Central File Exchange.
Oscarson, D.W., Huang, P.M., Liaw, W.K., Hammer, U.T., 1983. Kinetics of oxidation of arsenite by various manganese dioxides. Soil Sci. Soc. Am. J. 47 (4), 644–648.
Paikaray, S., Peiffer, S., 2022. Arsenic fractionation and mobilization in agricultural soils of NE Punjab, India. Appl. Geochem. 139, 105255.
Parfitt, R.L., Giltrap, D.J., Whitton, J.S., 1995. Contribution of organic-matter and clay-minerals to the cation-exchange capacity of soils. Commun. Soil Sci. Plant Anal. 26 (9–10), 1343–1355.
Parkhurst, D.L., Appelo, C.A.J., 2013. Modeling Techniques. Geological Survey, U.S, p. 497.
Pedersen, H.D., Postma, D., Jakobsen, R., 2006. Release of arsenic associated with the reduction and transformation of iron oxides. Geochim. Cosmochim. Acta 70 (16), 4116–4129.
Reich, T.J., Das, S., Koretsky, C.M., Lund, T.J., Landry, C.J., 2010. Surface complexation modeling of Pb(II) adsorption on mixtures of hydrous ferric oxide, quartz and kaolinite. Chem. Geol. 275 (3–4), 262–271.
Schwertmann, U., Wagner, F., Knicker, H., 2005. Ferrihydrite-humic associations: magnetic hyperfine interactions. Soil Sci. Soc. Am. J. 69 (4), 1009–1015.
Scott, M.J., Morgan, J.J., 1995. Reactions at oxide surfaces. 1. Oxidation of As(III) by synthetic birnessite. Environ. Sci. Technol. 29 (8), 1898–1905.
Silva, J., Mello, J.W.V., Gasparon, M., Abrahao, W.A.P., Ciminelli, V.S.T., Jong, T., 2010. The role of Al-Goethites on arsenate mobility. Water Res. 44 (19), 5684–5692.
Sjostedt, C., Persson, I., Hesterberg, D., Kleja, D.B., Borg, H., Gustafsson, J.P., 2013. Iron speciation in soft-water lakes and soils as determined by EXAFS spectroscopy and geochemical modelling. Geochim. Cosmochim. Acta 105, 172–186.
Smedley, P.L., Kinniburgh, D.G., 2002. A review of the source, behaviour and distribution of arsenic in natural waters. Appl. Geochem. 17 (5), 517–568.
Stevens, J.G., Khasanov, A., Miller, J.W., Pollak, H., Li, Z., 2005. Mössbauer Mineral Handbook. Mössbauer Effect Data Center, Asheville.

Stolze, L., Zhang, D., Guo, H.M., Rolle, M., 2019. Surface complexation modeling of arsenic mobilization from goethite: interpretation of an in-situ experiment. Geochim. Cosmochim. Acta 248, 274–288.
Suda, A., Makino, T., 2016. Functional effects of manganese and iron oxides on the dynamics of trace elements in soils with a special focus on arsenic and cadmium: a review. Geoderma 270, 68–75.
Tessier, A., Campbell, P.G.C., Bisson, M., 1979. Sequential extraction procedure for the speciation of particulate trace-metals. Anal. Chem. 51 (7), 844–851.
Tufano, K.J., Reyes, C., Saltikov, C.W., Fendorf, S., 2008. Reductive processes controlling arsenic retention: revealing the relative importance of iron and arsenic reduction. Environ. Sci. Technol. 42 (22), 8283–8289.
Wei, X., Ji, H.B., Wang, S.J., Chu, H.S., Song, C.S., 2014. The formation of representative lateritic weathering covers in south-central Guangxi (southern China). Catena 118, 55–72.
Wenzel, W.W., Kirchbaumer, N., Prohaska, T., Stingeder, G., Lombi, E., Adriano, D.C., 2001. Arsenic fractionation in soils using an improved sequential extraction procedure. Anal. Chim. Acta 436 (2), 309–323.
Xiao, J., Chen, W., Wang, L., Zhang, X.K., Wen, Y.B., Bostick, B.C., Wen, Y.L., He, X.H., Zhang, L.Y., Zhuo, X.X., Huang, K., Wang, N.T., Ji, J.F., Liu, Y.Y., 2022. New strategy for exploring the accumulation of heavy metals in soils derived from different parent materials in the karst region of southwestern China. Geoderma 417, 115806.
Zazzi, A., Jakobsson, A.-M., Wold, S., 2012. Ni(II) sorption on natural chlorite. Appl. Geochem. 27 (6), 1189–1193.
Zhang, L., Xiao, J., Ji, J., Liu, Y., 2021. Arsenate adsorption on different fractions of Iron oxides in the paddy soil from the karst region of China. Bull. Environ. Contam. Toxicol. 106 (1), 126–133.